

# Variational Inference for Gaussian Process Modulated Poisson Processes

Chris Lloyd\*  
Tom Gunter\*  
Michael A. Osborne  
Stephen J. Roberts

CLLOYD@ROBOTS.OX.AC.UK  
TGUNTER@ROBOTS.OX.AC.UK  
MOSB@ROBOTS.OX.AC.UK  
SJROB@ROBOTS.OX.AC.UK

Department of Engineering Science, University of Oxford

## Abstract

We present the first fully variational Bayesian inference scheme for continuous Gaussian-process-modulated Poisson processes. Such point processes are used in a variety of domains, including neuroscience, geo-statistics and astronomy, but their use is hindered by the computational cost of existing inference schemes. Our scheme: requires no discretisation of the domain; scales linearly in the number of observed events; and is many orders of magnitude faster than previous sampling based approaches. The resulting algorithm is shown to outperform standard methods on synthetic examples, coal mining disaster data and in the prediction of Malaria incidences in Kenya.

## 1. Introduction

Sparse events defined over a continuous domain arise in a variety of real-world applications. The geospatial spread of disease through time, for example, may be viewed as a set of infections which occur in three dimensional space-time. In this work, we will consider data where the intensity (or average incidence rate) of the event generating process is assumed to vary smoothly over the domain. A popular model for such data is the *inhomogenous Poisson process* with a *Gaussian process model* for the smoothly-varying intensity function. This flexible approach has been adopted for applications in neuroscience (Cunningham et al., 2008b), finance (Basu & Dassios, 2002) and forestry (Heikkinen & Arjas, 1999).

However, existing inference schemes for such models scale poorly with the number of data, preventing them from finding greater use. The use of a full Gaussian process in modelling the intensity (Adams et al., 2009) incurs prohibitive

$\mathcal{O}(N^3)$  computational scaling in the number of data points,  $N$ . To tackle this problem in practice, many approaches (Rathbun & Cressie, 1994; Miller et al., 1998) discretise the domain, binning counts within each segment. This approach enabled Cunningham et al. (2008a) to achieve  $\mathcal{O}(N \log N)$  performance. However, the discretisation approach suffers from poor scaling with the dimension of the domain and sensitivity to the choice of discretisation.

We introduce a new model for Gaussian-process-modulated Poisson processes that eliminates the requirement for discretisation, while simultaneously delivering  $\mathcal{O}(N)$  scaling. We further introduce the first fully variational Bayesian inference scheme for such models, allowing computation many orders of magnitude faster than existing schemes. This approach, which we term Variational Bayes for Point Processes (VBPP), is shown to provide more accurate prediction than benchmarks on held-out data from datasets including synthetic examples, coal mining disaster data and Malaria incidences in Kenya. The power of our approach suggests many future applications: in particular, our fully generative model will permit the joint inference of real-valued covariates (such as log-rainfall) and a point process (such as disease outbreaks).

## 2. Cox Processes

Formally a Cox process—a particular type of inhomogeneous Poisson process—is defined via a stochastic intensity function  $\lambda(\mathbf{x}) : \mathcal{X} \rightarrow \mathbb{R}^+$ . For a domain  $\mathcal{X} = \mathbb{R}^R$  of arbitrary dimension  $R$ , the number of points,  $N(\mathcal{T})$ , found in a subregion  $\mathcal{T} \subset \mathcal{X}$  is Poisson distributed with parameter  $\lambda_{\mathcal{T}} = \int_{\mathcal{T}} \lambda(\mathbf{x}) d\mathbf{x}$ —where  $d\mathbf{x}$  indicates integration with respect to the Lebesgue measure over the domain—and for disjoint subsets  $\mathcal{T}_i$  of  $\mathcal{X}$ , the counts  $N(\mathcal{T}_i)$  are independent. This independence is due to the completely independent nature of points in a Poisson process (Kingman, 1993).

If we restrict our consideration to some bounded region,  $\mathcal{T}$ , the probability density of a set of  $N$  observed points,

\* Corresponding authors.

$\mathcal{D} = \{\mathbf{x}^{(n)} \in \mathcal{T}\}_{n=1}^N$ , conditioned on the rate function  $\lambda(\mathbf{x})$  is

$$p(\mathcal{D} | \lambda) = \exp \left\{ - \int_{\mathcal{T}} \lambda(\mathbf{x}) d\mathbf{x} \right\} \prod_{n=1}^N \lambda(\mathbf{x}^{(n)}). \quad (1)$$

We use  $|\mathcal{T}|$  to denote the measure of the continuous domain  $\mathcal{T}$ . In this work we will assume  $\mathcal{T}$  is a hyper-rectangular sub-set of  $\mathbb{R}^R$  with boundaries  $\mathcal{T}_r^{\min}$  and  $\mathcal{T}_r^{\max}$  in each dimension  $r$  and

$$|\mathcal{T}| = \int_{\mathcal{T}} 1 d\mathbf{x} = \prod_{r=1}^R (\mathcal{T}_r^{\max} - \mathcal{T}_r^{\min}). \quad (2)$$

Using Bayes' rule, the posterior distribution of the rate function conditioned on the data,  $p(\lambda | \mathcal{D})$ , is

$$\frac{p(\lambda) \exp \left\{ - \int_{\mathcal{T}} \lambda(\mathbf{x}) d\mathbf{x} \right\} \prod_{n=1}^N \lambda(\mathbf{x}^{(n)})}{\int p(\lambda) \exp \left\{ - \int_{\mathcal{T}} \lambda(\mathbf{x}) d\mathbf{x} \right\} \prod_{n=1}^N \lambda(\mathbf{x}^{(n)}) d\lambda} \quad (3)$$

which is often described as ‘‘doubly-intractable’’ because of the nested integral in the denominator.

### 2.1. Inferring Intensity Functions

To overcome the challenges posed by the doubly intractable integral Adams et al. (2009) propose the Sigmoidal Gaussian Cox Process (SGCP). In the SGCP, a Gaussian process (Rasmussen & Williams, 2006) is used to construct an intensity function prior by passing a random function,  $f \sim \mathcal{GP}$ , through a sigmoid transformation and scaling it with a maximum intensity  $\lambda^*$ . The intensity function is therefore  $\lambda(x) = \lambda^* \sigma(f(x))$ , where  $\sigma(\cdot)$  is the logistic sigmoid (squashing) function

$$\sigma(x) = \frac{1}{1 + \exp(-x)}. \quad (4)$$

To remove the inner intractable integral, the authors augment the variable set to include latent data, such that the joint distribution of the latent and observed data is uniform Poisson over the region  $\mathcal{T}$ . While this model works well in practice on small, sparse event data in one dimension, in reality, it scales poorly with both the dimensionality of the domain and the maximum observed density of points. This is due to: the incorporation of latent, or thinned, data, whose number grows exponentially with the dimensionality of the space; and an  $\mathcal{O}(N^3)$  cost in the number  $N$  of all data (thinned or otherwise).

In Gunter et al. (2014a), the authors go some way towards improving the scalability of the SGCP, by introducing a further set of latent variables such that the entire space need no longer be thinned uniformly. Instead, they thin to a piecewise uniform Poisson process, maintaining the tractability of the inner integral, and allowing the model to scale to

higher dimensional point processes. The authors term this approach ‘‘adaptive thinning’’.

In Lasko (2014) the author performs renewal process inference without thinning the domain, by making use of a positively transformed intensity function. The intractability of their chosen approach forces them to resort to numerical integration techniques, however, and Bayesian inference is still performed using computationally expensive sampling.

### 3. Model

We construct our prior over the rate function using a Gaussian process. Rather than using a squashing function, we will assume<sup>1</sup> the intensity function is simply defined as  $\lambda(\mathbf{x}) = f^2(\mathbf{x})$ ,  $\mathbf{x} \in \mathcal{T}$ , where  $f$  is a Gaussian process distributed random function achieving a non-negative prior (Gunter et al., 2014b). Furthermore we will assume that  $f$  is dependent on a set of *inducing* points  $\mathcal{Z} = \{\mathbf{z}^{(m)} \in \mathcal{T}\}_{m=1}^M$ . We denote the evaluation of  $f$  at these points  $\mathbf{u}$ , and note  $\mathbf{u}$  has distribution  $\mathbf{u} \sim \mathcal{N}(\bar{\mathbf{1}}\bar{u}, \mathbf{K}_{zz})$ . Using this formulation  $f|\mathbf{u} \sim \mathcal{GP}(\mu(\mathbf{x}), \Sigma(\mathbf{x}, \mathbf{x}'))$  has mean and covariance functions

$$\mu(\mathbf{x}) = \mathbf{k}_{xz} \mathbf{K}_{zz}^{-1} \mathbf{u}, \quad (5)$$

$$\Sigma(\mathbf{x}, \mathbf{x}') = \mathbf{K}_{xx'} - \mathbf{k}_{xz} \mathbf{K}_{zz}^{-1} \mathbf{k}_{zx'}, \quad (6)$$

where  $\mathbf{k}_{xz}$ ,  $\mathbf{K}_{xx'}$ ,  $\mathbf{K}_{zz}$  are matrices evaluated at  $\mathbf{x}$ ,  $\mathbf{x}'$  and  $\mathcal{Z}$  using an appropriate kernel. We use the exponentiated quadratic (also known as the ‘‘squared exponential’’) ARD kernel

$$K(\mathbf{x}, \mathbf{x}') = \gamma \prod_{r=1}^R \exp \left( - \frac{(x_r - x'_r)^2}{2\alpha_r} \right). \quad (7)$$

With this hierarchical formulation the joint distribution over  $\mathcal{D}$ ,  $f$ ,  $\mathbf{u}$  and  $\Theta$  is

$$p(\mathcal{D}, f, \mathbf{u}, \Theta) = p(\mathcal{D} | \lambda = f^2) p(f | \mathbf{u}, \Theta) p(\mathbf{u} | \Theta) p(\Theta), \quad (8)$$

where  $p(\Theta)$  is an optional prior on the set of model parameters  $\Theta = \{\gamma, \alpha_1, \dots, \alpha_R, \bar{u}\}$ . For notational convenience we will often omit conditioning on  $\Theta$ .

### 4. Inference

We will use variational inference to obtain a bound on the model evidence  $p(\mathcal{D})$ . To achieve this we must integrate out  $f$  and  $\mathbf{u}$ , but we must also integrate  $f^2$  over the region  $\mathcal{T}$  due to the integral embedded in the likelihood, Equation 1.

<sup>1</sup>See Section 5 for a detailed motivation of this choice.

#### 4.1. Variational Bound

We begin by integrating out the inducing variables  $\mathbf{u}$ , using a variational distribution  $q(\mathbf{u}) = \mathcal{N}(\mathbf{u}; \mathbf{m}, \mathbf{S})$  over the inducing points. We now multiply and divide the joint by  $q(\mathbf{u})$  and lower bound using Jensen's inequality to obtain a lower bound on the model evidence:

$$\begin{aligned} \log p(\mathcal{D}|\Theta) &= \log \left[ \iint p(\mathcal{D}|\mathbf{f}) p(\mathbf{f}|\mathbf{u}) p(\mathbf{u}) \frac{q(\mathbf{u})}{q(\mathbf{u})} d\mathbf{u} d\mathbf{f} \right] \\ &\geq \iint p(\mathbf{f}|\mathbf{u}) q(\mathbf{u}) d\mathbf{u} \log[p(\mathcal{D}|\mathbf{f})] d\mathbf{f} \\ &\quad + \iint p(\mathbf{f}|\mathbf{u}) q(\mathbf{u}) d\mathbf{f} \log \left[ \frac{p(\mathbf{u})}{q(\mathbf{u})} \right] d\mathbf{u} \\ &= \mathbb{E}_{q(f)} [\log p(\mathcal{D}|\mathbf{f})] - \text{KL}(q(\mathbf{u})||p(\mathbf{u})) \\ &\triangleq \mathcal{L} \end{aligned} \quad (9)$$

Since  $p(\mathbf{f}|\mathbf{u})$  is conjugate to  $q(\mathbf{u})$ , we can write down in closed-form the resulting integral:

$$q(f) = \int p(\mathbf{f}|\mathbf{u}) q(\mathbf{u}) d\mathbf{u} = \mathcal{GP}(f; \tilde{\mu}, \tilde{\Sigma}), \quad (10)$$

$$\tilde{\mu}(\mathbf{x}) = \mathbf{k}_{xz} \mathbf{K}_{zz}^{-1} \mathbf{m},$$

$$\tilde{\Sigma}(\mathbf{x}, \mathbf{x}') = \mathbf{K}_{xx'} - \mathbf{k}_{xz} \mathbf{K}_{zz}^{-1} \mathbf{k}_{zx'} + \mathbf{k}_{xz} \mathbf{K}_{zz}^{-1} \mathbf{S} \mathbf{K}_{zz}^{-1} \mathbf{k}_{zx'}.$$

$\text{KL}(q(\mathbf{u})||p(\mathbf{u}))$  is simply the KL-divergence between two Gaussians

$$\begin{aligned} \text{KL}(q(\mathbf{u})||p(\mathbf{u})) &= \frac{1}{2} \left[ \text{tr}(\mathbf{K}_{zz}^{-1} \mathbf{S}) - \log \frac{|\mathbf{K}_{zz}|}{|\mathbf{S}|} - M \right. \\ &\quad \left. + (\tilde{\mathbf{u}} - \mathbf{m})^\top \mathbf{K}_{zz}^{-1} (\tilde{\mathbf{u}} - \mathbf{m}) \right]. \end{aligned} \quad (11)$$

We can now take expectations of the data log-likelihood under  $q(f)$ :

$$\begin{aligned} \mathcal{L} &= \mathbb{E}_{q(f)} [\log p(\mathcal{D}|\mathbf{f})] - \text{KL}(q(\mathbf{u})||p(\mathbf{u})) \\ &= \mathbb{E}_{q(f)} \left[ - \int_{\mathcal{T}} f_x^2 d\mathbf{x} + \sum_{n=1}^N \log f_n^2 \right] \\ &\quad - \text{KL}(q(\mathbf{u})||p(\mathbf{u})) \\ &= - \int_{\mathcal{T}} \{ \mathbb{E}_{q(f)} [f_x]^2 + \text{Var}_{q(f)} [f_x] \} d\mathbf{x} \\ &\quad + \sum_{n=1}^N \mathbb{E}_{q(f)} [\log f_n^2] - \text{KL}(q(\mathbf{u})||p(\mathbf{u})), \end{aligned} \quad (12)$$

where to keep the notation concise we have introduced the following identities:

$$\begin{aligned} f_x &\triangleq f(\mathbf{x}), & \tilde{\mu}_x &\triangleq \tilde{\mu}(\mathbf{x}), & \tilde{\sigma}_x^2 &\triangleq \tilde{\Sigma}(\mathbf{x}, \mathbf{x}), \\ f_n &\triangleq f(\mathbf{x}^{(n)}), & \tilde{\mu}_n &\triangleq \tilde{\mu}(\mathbf{x}^{(n)}), & \tilde{\sigma}_n^2 &\triangleq \tilde{\Sigma}(\mathbf{x}^{(n)}, \mathbf{x}^{(n)}). \end{aligned}$$

Note we have used Tonelli's Theorem to reverse the ordering of the integrations over the positive integrand  $f_x^2 q(f)$ . We now have two tasks remaining: we must compute the integral over the region  $\mathcal{T}$  and calculate the expectations  $\mathbb{E}_{q(f)} [\log f_n^2]$  at the data points.

#### 4.2. Integrating Over The Region $\mathcal{T}$

This lower bound has the desirable property that we can take expectations under  $q(f)$  at any specific point,  $\mathbf{x}$ , of the function value,  $f(\mathbf{x})$ , since  $q(f(\mathbf{x}))$  is Gaussian. It is only possible to take useful expectations because: a) we used the conditional GP formulation, allowing tractable expectations to be taken w.r.t.  $q(f)$ ; b), we have already integrated out the inducing variables  $\mathbf{u}$ ; and c) we chose a suitable transformation, i.e.  $\lambda(\mathbf{x}) = f^2(\mathbf{x})$ .

The required statistics for Equation 12 are:

$$\mathbb{E}_{q(f)} [f_x]^2 = \tilde{\mu}_x^2 = \mathbf{m}^\top \mathbf{K}_{zz}^{-1} \mathbf{k}_{xz} \mathbf{k}_{xz} \mathbf{K}_{zz}^{-1} \mathbf{m}, \quad (13)$$

$$\begin{aligned} \text{Var}_{q(f)} [f_x] &= \tilde{\sigma}_x^2 = \mathbf{k}_{xx} - \text{Tr}(\mathbf{K}_{zz}^{-1} \mathbf{k}_{xz} \mathbf{k}_{xz}) \\ &\quad + \text{Tr}(\mathbf{K}_{zz}^{-1} \mathbf{S} \mathbf{K}_{zz}^{-1} \mathbf{k}_{xz} \mathbf{k}_{xz}). \end{aligned} \quad (14)$$

It is now easy to calculate the integral since only  $\mathbf{k}_{zx} = \mathbf{k}_{xz}^\top$  is a function of  $\mathbf{x}$ , leading to the following terms:

$$\int_{\mathcal{T}} \mathbb{E}_{q(f)} [f_x]^2 d\mathbf{x} = \mathbf{m}^\top \mathbf{K}_{zz}^{-1} \Psi \mathbf{K}_{zz}^{-1} \mathbf{m}, \quad (15)$$

$$\begin{aligned} \int_{\mathcal{T}} \text{Var}_{q(f)} [f_x] d\mathbf{x} &= \gamma |\mathcal{T}| - \text{Tr}(\mathbf{K}_{zz}^{-1} \Psi) \\ &\quad + \text{Tr}(\mathbf{K}_{zz}^{-1} \mathbf{S} \mathbf{K}_{zz}^{-1} \Psi). \end{aligned} \quad (16)$$

For the exponentiated quadratic ARD kernel, the matrix

$$\Psi = \int K(\mathbf{z}, \mathbf{x}) K(\mathbf{x}, \mathbf{z}') d\mathbf{x} \quad (17)$$

can be calculated by re-arranging the product as a single exponentiated quadratic in  $\mathbf{x}$  and  $\bar{\mathbf{z}}$  as follows:

$$\begin{aligned} \Psi(\mathbf{z}, \mathbf{z}') &= \int_{\mathcal{T}} \gamma^2 \prod_{r=1}^R \exp \left( - \frac{(z_r - z'_r)^2}{4\alpha_r} - \frac{(x_r - \bar{z}_r)^2}{\alpha_r} \right) d\mathbf{x} \\ &= \gamma^2 \prod_{r=1}^R - \frac{\sqrt{\pi\alpha_r}}{2} \exp \left( - \frac{(z_r - z'_r)^2}{4\alpha_r} \right) \\ &\quad \times \left[ \text{erf} \left( \frac{\bar{z}_r - \mathcal{T}_r^{\max}}{\sqrt{\alpha_r}} \right) - \text{erf} \left( \frac{\bar{z}_r - \mathcal{T}_r^{\min}}{\sqrt{\alpha_r}} \right) \right], \end{aligned}$$

where  $\bar{\mathbf{z}} = [\bar{z}_1, \dots, \bar{z}_R]^\top$  has elements  $\bar{z}_r = \frac{z_r + z'_r}{2}$ .

In addition to the exponentiated quadratic ARD kernel, the matrix  $\Psi$  can be computed in closed-form for other kernels, including polynomial and periodic kernels, as well as sum and product combinations of kernels.

#### 4.3. Expectations At The Data Points

The expectation  $\mathbb{E}_{q(f)} [\log f_n^2]$  has an analytical—albeit complicated—solution expressed as

$$\mathbb{E}_{q(f)} [\log f_n^2] = \int_{-\infty}^{\infty} \log(f_n^2) \mathcal{N}(f_n, \tilde{\mu}_n, \tilde{\sigma}_n^2) df_n \quad (18)$$

$$= -\tilde{G} \left( -\frac{\tilde{\mu}_n^2}{2\tilde{\sigma}_n^2} \right) + \log \left( \frac{\tilde{\sigma}_n^2}{2} \right) - C, \quad (19)$$

where  $C \approx 0.57721566$  is the Euler-Mascheroni constant and  $\tilde{G}$  is defined via the confluent hyper-geometric function

$${}_1F_1(a, b, z) = \sum_{k=0}^{\infty} \frac{(a)_k z^k}{(b)_k k!}, \quad (20)$$

where  $(\cdot)_k$  denotes the rising Pochhammer series

$$(a)_0 = 1, \quad (a)_k = a(a+1)(a+2)\dots(a+k-1).$$

Specifically  $\tilde{G}$  is a specialised version of the partial derivative of  ${}_1F_1$  with respect to its first argument and can be computed using the method of Ancarani & Gasaneo (2008), which has a particular solution at  $a = 0$ , leading to the following definition of  $\tilde{G}$ :

$$\tilde{G}(z) = {}_1F_1^{(1,0,0)}\left(0, \frac{1}{2}, z\right) = 2z \sum_{j=0}^{\infty} \frac{j! z^j}{(2)_j (1\frac{1}{2})_j}. \quad (21)$$

Naive implementation of Equation 21 has poor numerical stability, although this can be improved somewhat using an iterative scheme, in practice we therefore use a large multi-resolution look-up table of precomputed values obtained from a numerical-package. As shown in Figure 1, this function decreases very slowly as its argument becomes increasingly negative, so we can easily compute accurate evaluations of  $\tilde{G}(z)$  for any  $z$  by linear interpolation of our lookup table and, as a by-product, we also obtain  $\tilde{G}'$ .

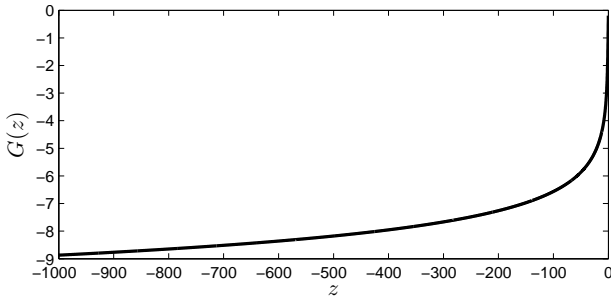


Figure 1. Accurate evaluations of  $\tilde{G}$  can be obtained from a pre-computed look-up table.

#### 4.4. Optimising The Bound

To perform inference we find variational parameters  $\mathbf{m}^*$ ,  $\mathbf{S}^*$  and the model parameters  $\Theta^*$  that maximise  $\mathcal{L}$ . To optimise these simultaneously we construct an augmented vector  $\mathbf{y} = [\Theta^\top, \mathbf{m}^\top, \text{vech}(\mathbf{L})^\top]^\top$ —where  $\text{vech}(\mathbf{L})$  is the vectorisation of the lower triangular elements of  $\mathbf{L}$ , such that  $\mathbf{S} = \mathbf{L}\mathbf{L}^\top$ .

As well as the maximum-likelihood solution, we can also compute the the maximum-a-posterior (MAP) estimate by maximising  $\mathcal{L}(\mathcal{D}; \mathbf{y}) + \log p(\Theta)$ .

To optimise the inducing point locations we use the change of variables

$$z_r^{(m)} = \frac{\mathcal{T}_r^{\min} + \mathcal{T}_r^{\max}}{2} - \frac{\mathcal{T}_r^{\min} - \mathcal{T}_r^{\max}}{2} \sin(\omega_r^{(m)}), \quad (22)$$

and optimise in  $\omega_r^{(m)} \in [-\pi, \pi]$ , which ensures the inducing points always remain within the region  $\mathcal{T}$ .

#### 4.5. Locating The Inducing Points

One final part of our model we have so far left unspecified is the number and location of inducing points. In principle, for a given set of parameters  $\Theta$ , we will obtain a lower bound for the true GP likelihood for any number of inducing points in any configuration of locations. We consider two possible approaches: firstly, treating the inducing points as optimisation parameters and, secondly, fixing them on a regular grid.

If the locations of the inducing points are optimised, this suggests—in common with other sparse GP models—that we can achieve good performance using a small number of well-placed inducing points. This is achieved at the cost of an additional set of optimisation parameters, although the size of  $\mathbf{m}$  and  $\mathbf{S}$  are commensurately reduced. Optimisation of the inducing points is particularly computationally expensive, however, because of the necessity to recompute  $\mathbf{K}_{zz}^{-1}$  for each dimension of each inducing point ( $M \times R$  in total) and since  $\mathbf{K}_{zz}$  affects every term in the bound.

Regular grids, on the other hand, also have several advantages. Consider firstly that—in contrast to standard sparse GP regression—the accuracy of our solution is not only governed by the distance between the inducing points and the data points. The variance of  $f(\mathbf{x})$  increases as  $\mathbf{x}$  becomes further from the inducing points. However, the rate function,  $\lambda$ , is a function of both the mean *and* the variance of  $f$ . Since we are integrating  $\lambda$  over  $\mathcal{T}$ , we need inducing points distributed across  $\mathcal{T}$  and not just in regions close to the data. An evenly-spaced grid is one way to ensure this is achieved.

Regularly sampled grids also afford potential computational advantages. When the grid points are evenly spaced, the kernel matrix has Toeplitz structure, and hence allows matrix inversion (and linear solving) in  $\mathcal{O}(M \log^2 M)$  time, a fact previously utilised for efficient point processes by Cunningham et al. (2008a). Furthermore, when the kernel function is separable across the dimensions (as specified by Equation (7)), the kernel matrix has Kronecker structure which can further reduce the cost of matrix inversion (Osborne et al., 2012). The latter is relevant to all sparse GP applications based on inducing points, however, it is particularly relevant for this application as we are motivated by the doubly intractable nature of Equation 3. In our implementation, we use naïve inversion of the induc-

ing point kernel matrix,  $\mathbf{K}_{zz}$ , resulting in computational complexity of  $\mathcal{O}(NM^3)$ . Hence the computation times reported below could be improved with a relatively small amount of additional implementation effort.

#### 4.6. Predictive Distribution

To form the predictive distribution we assume our optimised variational distribution  $q^*(\mathbf{u}) = \mathcal{N}(\mathbf{u}; \mathbf{m}^*, \mathbf{S}^*)$  approximates the posterior  $p(\mathbf{u}|\mathcal{D})$ . Analogously to Equation 10 we next compute  $q^*(f) \approx p(f|\mathcal{D})$ . We can now derive a lower bound of the (approximate) predictive log-likelihood on a held-out test dataset  $\mathcal{H}$ :

$$\begin{aligned} \log p(\mathcal{H}|\mathcal{D}, \Theta^*) &= \log \mathbb{E}_{p(f|\mathcal{D})} [p(\mathcal{H}|f)] \\ &\approx \log \mathbb{E}_{q^*(f)} [p(\mathcal{H}|f)] \triangleq \mathcal{M}_p \\ &\geq \mathbb{E}_{q^*(f)} [\log p(\mathcal{H}|f)] \triangleq \mathcal{L}_p. \end{aligned} \quad (23)$$

The derivation of  $\mathcal{L}_p$  follows Equations 12-19. The resulting bound is the same as  $\mathcal{L}$  except  $\mathbf{m}$ ,  $\mathbf{S}$  are replaced with  $\mathbf{m}^*$  and  $\mathbf{S}^*$ , and there is no KL divergence term. Kernel matrices are computed using  $\Theta^*$ .

The tightness of this final bounding step will be a function of how well the inducing variables  $\mathbf{u}$  define the function  $f$ . Intuitively, when the variance at the inducing points is large, the entropy of  $f$  will be large, as it is unrestricted. From an information theoretic perspective, we can say that the tightness of the bound will be a function of the entropy of  $f$ :  $H(f) = \frac{1}{2} \log |\tilde{\Sigma}| + \text{const.}$

Given this knowledge we define a second, tightened, lower bound  $\mathcal{L}_0$ , where we allow the variance of function values at the inducing points to collapse to zero:  $p(\mathbf{u}|\mathcal{D}) \approx \delta(\mathbf{m})$ . This reduces the conditional entropy of  $f$  given  $\mathbf{u}$  by shrinking the final term in the definition of  $\tilde{\Sigma}$  (Equation 10), resulting in a tighter bound for a slightly restricted class of models. As it is a slightly more restricted model, we expect the ground truth  $\mathcal{M}_0 = \log (\mathbb{E}_{q(f|\mathbf{u}=\mathbf{m})} [p(\mathcal{H}|f)])$  to be lower than the ground truth  $\mathcal{M}_p$ . In practice, however, because the variational  $\mathcal{L}_0$  is so much tighter, we also use this to give results for approximate predictive likelihood when comparing against other approaches. In Figure 7 we demonstrate this empirically for the coal mining dataset by evaluating the true predictive bounds on a held-out 50% of the data via 10,000 MCMC samples, and shading between these and the variational approximations. We do this for a range of inducing point grid densities, both with and without optimisation of the inducing point locations. In Figures 6, 5, and 7, we plot all of the bounds described above as the number of inducing points increase. We note that for the relatively smooth coal mining data, (Figure 7), all bounds do not benefit from more than about 10 inducing points, while in the case of the twitter data, the faster dynamics call for increased numbers. In all Figures the tightness of  $\mathcal{L}_0$  is evident as compared to  $\mathcal{L}_p$ .

## 5. Alternative GP Transformations

At this point it is worth considering why we have chosen the function transformation  $\lambda(\mathbf{x}) = f^2(\mathbf{x})$  in preference to other alternatives we might have used. An obvious first choice would be

$$\lambda(\mathbf{x}) = \exp(f(\mathbf{x})). \quad (24)$$

This transformation is undesirable for two reasons. The more obvious of these is that after taking expectations under  $q(f)$  we are left with the integral

$$- \int_{\mathcal{T}} \exp \left( \tilde{\mu}_x + \frac{\tilde{\sigma}_x^2}{2} \right) d\mathbf{x}, \quad (25)$$

which cannot be computed in closed form. We could approximate the integral using a series expansion, however this would be difficult with more than a couple of terms and furthermore, since the function is concave, this approximation would not be a lower bound.

The second—and more subtle—reason is that in using this transformation, when we take expectations under  $q(f)$  of the data, we obtain

$$\mathbb{E}_{q(f)} [\log \{\exp(f_n)\}] = \tilde{\mu}_n. \quad (26)$$

Since the mean,  $\tilde{\mu}_n$ , is not a function of  $\mathbf{S}$ , the variance of the variational distribution  $q(\mathbf{u})$ , we have effectively decoupled the data from the uncertainty on our variational approximation; this is clearly undesirable.

Another possible candidate is the probit function,  $\lambda(x) = \Phi(f(x))$ . This can be integrated analytically against the GP prior, however we are again left with a difficult integral over  $\mathcal{T}$  which is

$$- \int_{\mathcal{T}} \Phi \left( \frac{\tilde{\mu}_x}{\sqrt{1 + \tilde{\sigma}_x^2}} \right) d\mathbf{x}. \quad (27)$$

As the range of this transformation is  $(0, 1)$  we would also require additional machinery to infer a scaling variable.

In contrast the square transform presented allows the integral over the region  $\mathcal{T}$  to be computed in closed form and  $\mathbb{E}_{q(f)} [\log f_n^2]$  can be computed quickly and accurately. Importantly this transformation also maintains the connection between the data and the variational uncertainty.

Although the square transform is not a one-to-one function—any rate function  $\lambda$  may have been generated by  $f^2$  or  $(-f)^2$ —this sign ambiguity is integrated out in a Bayesian sense, Equation 18.

## 6. Relationship to Sparse GP Models

The use of inducing points in our model relates it to a wide range of sparse Gaussian process models, e.g. SPGP (Snelson & Ghahramani, 2005). The variational sparse Gaussian

process framework was introduced by Titsias (2009), however the bound we develop is more akin to the “Big-Data” GP bound (Hensman et al., 2013), since we explicitly maintain the variational distribution  $q(\mathbf{u})$ . The variable  $\Psi$  that results from integrating the kernel over the input domain is similar to the so-called “ $\Psi$ -statistic” which arises when integrating out the uncertainty of latent variables in the variational GPLVM (Titsias & Lawrence, 2010).

## 7. Experiments

To evaluate our algorithm, we benchmarked against our frequentist kernel smoothing approach, described below, both with and without end correction (KS+EC and KS-EC respectively), and a fully Bayesian SGCP MCMC sampler. Our test data sets are generative data from the SGCP model and several real-world data sets.

### 7.1. Benchmarks

Our kernel smoothing method is similar to standard kernel density estimation except we use truncated normal kernels to account for our explicit knowledge of the domain—the latter is referred to as “end-correction” in some literature (Diggle, 1985). The kernel smoother optimises a diagonal covariance,  $\Sigma^*$ , by maximising the leave-one-out training objective

$$\Sigma^* = \operatorname{argmax}_{\Sigma} \sum_{i=1}^N \log \sum_{j \neq i=1}^N \mathcal{N}_{\mathcal{T}}(\mathbf{x}^{(i)}; \mathbf{x}^{(j)}, \Sigma). \quad (28)$$

We can construct the predictive distribution by combining the maximum-likelihood estimates of the size and spatial location of the data. For a test data set  $\mathcal{H}$  (with  $K!$  permutations) this distribution is

$$p(\mathcal{H}|\mathcal{D}) = K! p(K|\mathcal{D}) \prod_{k=1}^K p(\tilde{\mathbf{x}}^{(k)}|\mathcal{D}), \quad (29)$$

where the location density,

$$p(\tilde{\mathbf{x}}^{(k)}|\mathcal{D}) = \frac{1}{N} \sum_{n=1}^N \mathcal{N}_{\mathcal{T}}(\tilde{\mathbf{x}}^{(k)}; \mathbf{x}^{(n)}, \Sigma^*), \quad (30)$$

is computed using the previously described method and the distribution of the number of points,

$$p(K|\mathcal{D}) = \frac{N^K}{K!} \exp(-N), \quad (31)$$

is simply a Poisson distribution with parameter  $N$ . It is straight forward to show that Equation 29 is equivalent to Equation 1 since we can interpret the rate function as  $\lambda(\mathbf{x}) = \sum_{n=1}^N \mathcal{N}_{\mathcal{T}}(\mathbf{x}; \mathbf{x}^{(n)}, \Sigma^*)$  and since  $\int_{\mathcal{T}} \lambda(\mathbf{x}) d\mathbf{x} = N$ .

Our SGCP sampler is based on Adams et al. (2009). Our implementation differs by using elliptical slice sampling to infer the latent function  $f$  and we perform hyper-parameter inference using Hybrid Monte-Carlo (HMC). We also use the “adaptive-thinning” method described in Gunter et al. (2014a), to reduce the number of thinning points required.

### 7.2. Synthetic Data

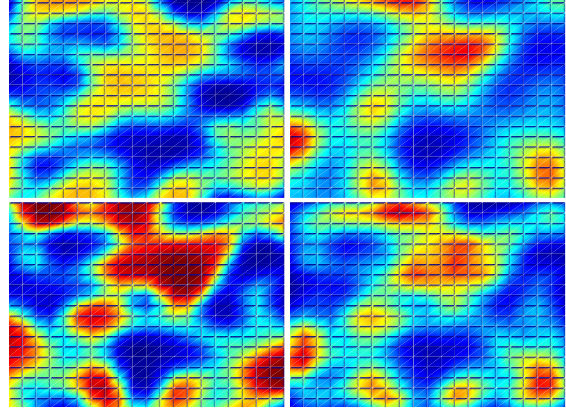


Figure 2. 2D Synthetic Data. Clockwise from top left: Ground truth, VBPP, KS+EC, SGCP.

For the synthetic data sets, we first generate a 2D function from a high resolution grid using a Gaussian process and sigmoid link function, and then, conditioned on that function, we draw a training dataset and multiple test datasets. We give average performances results for these test datasets in Table 1. Figure 2 visualises an inferred 2D intensity conditioned on  $\sim 500$  observations. Although the SGCP sampler gives better predictive performance than the VBPP  $\mathcal{L}_0$  bound, it should be noted that the sampler uses well tuned hyper-parameters, uses the same link function as the generative process and is much more computationally expensive. VBPP outperforms kernel smoothing in terms of both predictive likelihood and RMS error.

### 7.3. Real Data

We next investigate three real world data sets. For these data sets we create training and test subsets by allocating each point to either subset with probability 0.5. Since true rates are unknown for these datasets we rely on held-out predictive likelihood as the only performance metric.

#### 7.3.1. COAL MINING DISASTER DATA

Our first real dataset comprises 190 events recorded from March 15, 1851 to March 22, 1962; each represents a coal-mining disaster that killed at least ten people in the United Kingdom. These data, first analysed in this form in 1979 (Jarrett, 1979), have often been tackled with nonhomoge-

Table 1. Results for 2D synthetic data (drawn from the SGCP generative process).

Function	SGCP			KS+EC			VBPP ( $\mathcal{L}_0$ )		
	Avg. LL	RMS	Time(s)	Avg. LL	RMS	Time(s)	Avg. LL	RMS	Time(s)
1	446.1	1.37	7547.83	389.8	1.48	0.34	392.9	1.21	3.26
2	-61.1	0.38	1039.65	-78.3	0.46	0.02	-76.1	0.38	2.00
3	122.4	0.88	3173.91	84.3	1.04	0.12	92.6	0.81	2.44
4	175.8	1.71	3773.75	147.0	1.26	0.05	148.3	1.14	2.58
5	446.1	2.94	6368.44	413.6	2.02	0.21	415.5	1.81	2.83

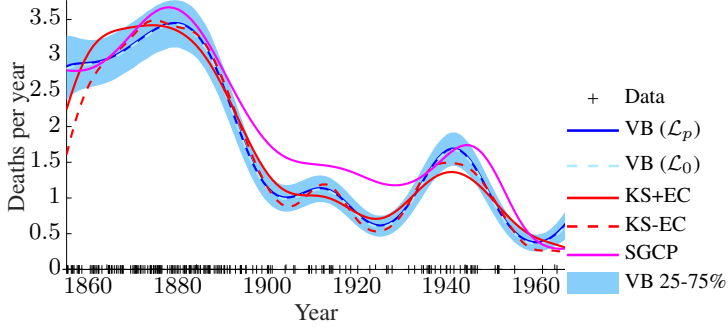


Figure 3. Coal mining disaster data.

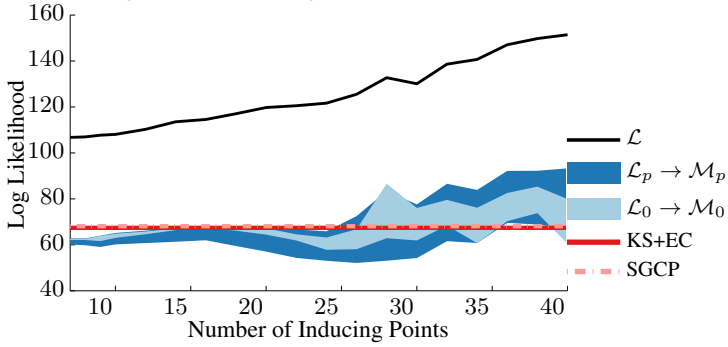


Figure 5. Twitter data (Z on a fixed grid).

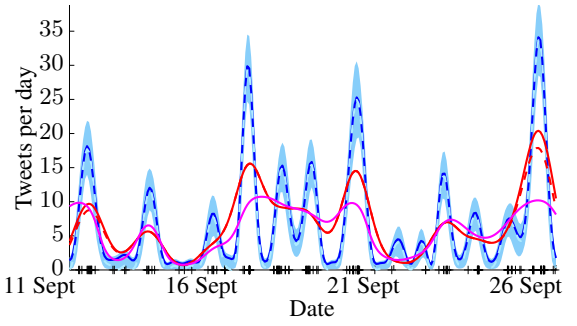


Figure 4. Twitter data

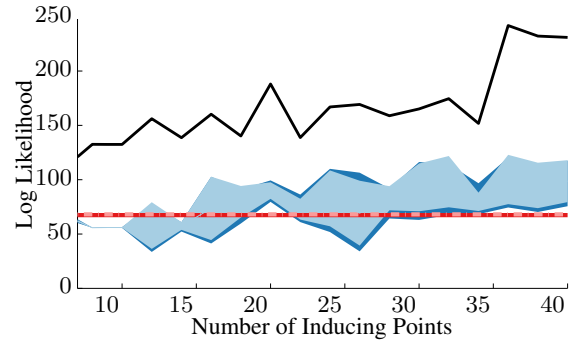


Figure 6. Twitter data (Z optimised).

neous Poisson processes, (Adams et al., 2009), as the rate of such disasters is expected to vary according to known historical developments. The events are indicated by the rug plot along the axis of Figure 3.

Our inferred intensity of disasters correlates with the historical introduction of safety regulation, as noted in previous work on this data (Fearnhead, 2006; Carlin et al., 1992). Firstly, our results depict a decline in the rate of such disasters throughout 1870–1890, a period that saw the UK parliament passing several acts with the aim of improving safety for mine workers, including the Coal Mines Regulation Acts of 1872 and 1887. Our inferred intensity also declines after 1950, likely related to the imposition of further safety regulation with the Mines and Quarries Act, 1954.

Predictive log-likelihood values on held out data (Figure 7) are also encouraging. VBPP outperforms kernel smoothing and SGCP with as few as 10 inducing points; more induc-

ing points yielding no further benefit.

### 7.3.2. TWITTER DATA

Next, we ran the models on the tweet profile of the chairman of the ‘Better Together Campaign’, Alistair Darling, one week either side of the Scottish independence election (189 tweets). Results are shown in Figure 4 and Table 2, where half the data was held out and a regular 31 point grid was used. Figures 5 and 6 compare the performance of regularly spaced and optimised inducing points, and show optimisation yields considerably improved performance on this dataset. The  $\mathcal{L}_0$  and  $\mathcal{L}_p$  bounds become less tight as the number of inducing points is increased, suggesting there is less uncertainty represented in the variational parameter  $\mathbf{S}$  and more uncertainty captured by a reduced kernel length scale. This transition is observed for fewer inducing points when inducing point optimisation is employed. Both with



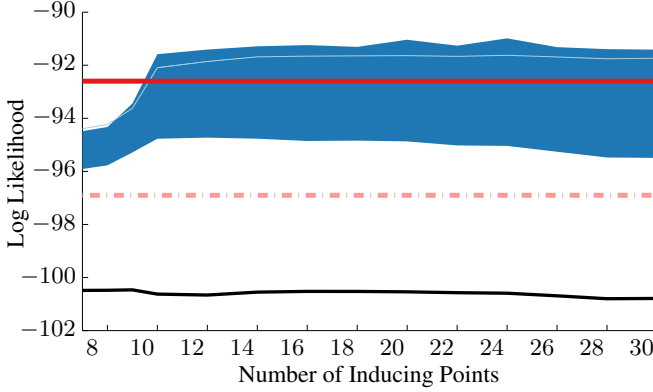


Figure 7. Coal Mining Data set: The difference between sampling  $\mathcal{M}_0$  and  $\mathcal{M}_p$ , and the corresponding lower bounds,  $\mathcal{L}_0$  and  $\mathcal{L}_p$  (see Section 4.6). The figure clearly demonstrates the tightness of the  $\mathcal{L}_0$  bound. Legend as in Figure 5.

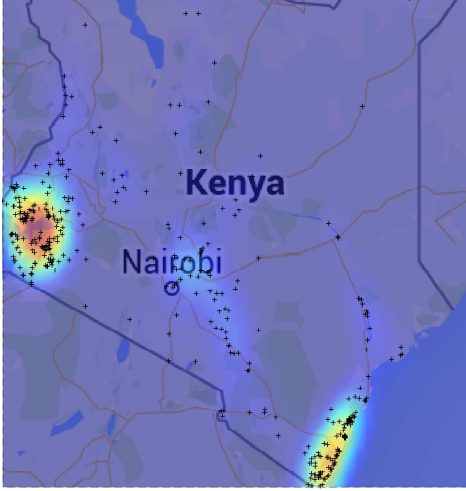


Figure 8. A sample of 741 malaria incidences in Kenya, which occurred over the course of 1985-2010, and the associated VBPP intensity function.  $20 \times 20$  inducing points.

and without inducing point optimisation, VBPP  $\mathcal{M}_0$  and  $\mathcal{M}_p$  outperform both the SGCP and kernel smoothing by a wide margin, suggesting the square link function is an appropriate model for this data.

### 7.3.3. MALARIA DATA

We expect that a major application of the contributions presented in this paper is the joint modelling of disease incidence with correlating factors, in a fully Bayesian, scalable framework. For example, those studying the spread of malaria often wish to use continuous rainfall measurements to better inform their epidemiological models. We use examples from the Malaria Atlas Project (2014) to test our scheme. We extracted 741 incidences of malaria outbreak documented in Kenya between 1985 and 2010, and ran our

VBPP algorithm and kernel smoothing on approximately half of the resulting dataset, holding out the remainder for testing. Test log-likelihood results, given in Table 3, show VBPP performs comparably to kernel smoothing.

Table 2. Run times for 1D data sets.

Method	Coal Mining	Twitter
VBPP	0.7	0.5
KS+EC	0.0	0.3
KS-EC	0.0	0.2
SGCP	417.6	230.0

Table 3. Test log-likelihood for 2D Malaria data.

KS-EC	KS+EC	VBPP( $\mathcal{M}_p$ )	VBPP( $\mathcal{L}_0$ )
855.0	867.2	869.7	855.9

## 8. Further Work

Although the performance of the variational Bayesian point process inference algorithm described in this paper improves upon standard methods when used in isolation, it is in its extensions that its utility will be fully realised. Previous work (Gunter et al., 2014a) has shown that hierarchical modelling of point processes—structured point processes—can significantly improve predictive accuracy. In these multi-output models, statistical strength is shared across multiple rate processes via shared latent processes. The method presented here provides a likelihood model for point-process data that can be incorporated as a probabilistic building-block into these larger interconnected models. That is, our fully generative model can readily be extended to additionally incorporate other observation modalities. For example, real-valued observations such as (log-) household income could be modelled along with the intensity function over crime incidents using a variational multi-output GP framework. Future work will be aimed towards developing these variational structured point process algorithms and integration of these techniques to popular Gaussian process tool-kits, such as GPy (The GPy authors, 2014).

## 9. Conclusion

Point process models have hitherto been hindered by their scaling with the number of data. To address this problem, we propose a new model, accommodating non-discretised intensity functions, that permits linear scaling. We additionally contribute a variational Bayesian inference scheme that delivers rapid and accurate prediction. The scheme is validated on real datasets including the canonical coal mining disaster data set and malaria incidence in Kenya data.



## ACKNOWLEDGEMENTS

The authors would like to thank James Hensman and Neil Lawrence for helpful discussions. Chris Lloyd is funded by a DSTL National PhD Scheme Studentship. Tom Gunter is supported by UK Research Councils.

## References

- Adams, R. P., Murray, I., and MacKay, D. J. C. Tractable Nonparametric Bayesian Inference in Poisson Processes with Gaussian Process Intensities. In *Proceedings of the 26th Annual International Conference on Machine Learning, ICML '09*, pp. 9–16, New York, NY, USA, 2009. ACM.
- Ancarani, L. U. and Gasaneo, G. Derivatives of any order of the confluent hypergeometric function  ${}_1F_1(a, b, z)$  with respect to the parameter  $a$  or  $b$ . *Journal of Mathematical Physics*, 49(6), 2008.
- Basu, S. and Dassios, A. A Cox process with log-normal intensity. *Insurance: Mathematics and Economics*, 31(2):297302, Oct 2002.
- Carlin, B. P., Gelfand, A. E., and Smith, A. F. M. Hierarchical Bayesian analysis of changepoint problems. *Journal of the Royal Statistical Society. Series C (Applied Statistics)*, 41(2):389405, Jan 1992.
- Cunningham, J. P., Shenoy, K. V., and Sahani, M. Fast Gaussian process methods for point process intensity estimation. In *Proceedings of the 25th international conference on Machine learning*, pp. 192–199. ACM, 2008a.
- Cunningham, J. P., Yu, B. M., Shenoy, K. V., and Sahani, M. Inferring neural firing rates from spike trains using Gaussian processes. In *Advances in Neural Information Processing Systems 20*, 2008b.
- Diggle, P. A kernel method for smoothing point process data. *Journal of the Royal Statistical Society. Series C (Applied Statistics)*, 34(2):pp. 138–147, 1985. ISSN 00359254.
- Fearnhead, P. Exact and efficient Bayesian inference for multiple changepoint problems. *Statistics and Computing*, 16(2):203213, Jun 2006.
- Gunter, T., Lloyd, C., Osborne, M. A., and Roberts, S. J. Efficient Bayesian nonparametric modelling of structured point processes. In *Uncertainty in Artificial Intelligence (UAI)*, 2014a.
- Gunter, T., Osborne, M. A., Garnett, R., Hennig, P., and Roberts, S. Sampling for inference in probabilistic models with fast Bayesian quadrature. In Cortes, C. and Lawrence, N. (eds.), *Advances in Neural Information Processing Systems (NIPS)*, 2014b.
- Heikkinen, J. and Arjas, E. Modeling a Poisson forest in variable elevations: A nonparametric Bayesian approach. *Biometrics*, 55(3):738745, Sep 1999.
- Hensman, J., Fusi, N., and Lawrence, N. D. Gaussian Processes for Big Data. *CoRR*, abs/1309.6835, 2013.
- Jarrett, R. G. A note on the intervals between coal-mining disasters. *Biometrika*, 66(1):191193, 1979.
- Kingman, J. F. C. *Poisson Processes (Oxford Studies in Probability)*. Oxford University Press, Jan 1993. ISBN 0198536933.
- Lasko, T. A. Efficient Inference of Gaussian Process Modulated Renewal Processes with Application to Medical Event Data. In *Uncertainty in Artificial Intelligence (UAI)*, 2014.
- Malaria Atlas Project. <http://www.map.ox.ac.uk/explore/data-modelling/>, 2014. [Online; accessed 24-October-2014].
- Miller, J., Syversveen, A. R., and Waagepetersen, R. P. Log Gaussian Cox Processes. *Scandinavian Journal of Statistics*, 25(3):451–482, 1998. ISSN 1467-9469.
- Osborne, M. A., Roberts, S. J., Rogers, A., and Jennings, N. R. Real-time information processing of environmental sensor network data. *ACM Transactions on Sensor Networks*, 9(1), 2012.
- Rasmussen, C. E. and Williams, C. K. I. *Gaussian Processes for Machine Learning*. The MIT Press, 2nd edition 2006 edition, 2006. ISBN 0-262-18253-X.
- Rathbun, S. L. and Cressie, N. Asymptotic properties of estimators for the parameters of spatial inhomogeneous Poisson point processes. *Advances in Applied Probability*, pp. 122154, 1994.
- Snelson, E. and Ghahramani, Z. Sparse Gaussian Processes using Pseudo-inputs. In *Advances in Neural Information Processing Systems (NIPS)*, 2005.
- The GPy authors. GPy: A Gaussian process framework in Python. <https://github.com/SheffieldML/GPy>, 2014.
- Titsias, M. K. Variational Learning of Inducing Variables in Sparse Gaussian Processes. In *Artificial Intelligence and Statistics 12*, 2009.
- Titsias, M. K. and Lawrence, N. D. Bayesian Gaussian process latent variable model. In *Artificial Intelligence and Statistics 10*, 2010.